Influence of Masonry Infills on Seismic Performance of an Existing RC Building Retrofitted by Means of FPS Devices

applied sciences

MDPI

Article

Influence of masonry infills on seismic performance of an existing RC building retrofitted by means of FPS devices

Diego Gino[1], Elena Miceli[2,*], Luca Giordano[3], Giuseppe Carlo Marano[4] and Paolo Castaldo[5]

[1] Politecnico di Torino, Corso Duca degli Abruzzi 24, 1029, Turin, Italy; diego.gino@polito.it
[2] Politecnico di Torino, Corso Duca degli Abruzzi 24, 1029, Turin, Italy; elena.miceli@polito.it
[3] Politecnico di Torino, Corso Duca degli Abruzzi 24, 1029, Turin, Italy; luca.giordano@polito.it
[4] Politecnico di Torino, Corso Duca degli Abruzzi 24, 1029, Turin, Italy; giuseppe.marano@polito.it
[5] Politecnico di Torino, Corso Duca degli Abruzzi 24, 1029, Turin, Italy; paolo.castaldo@polito.it
* Correspondence: elena.miceli@polito.it; Tel.: +39 0110905305

Abstract: The safety assessment of existing structures in areas with a relevant seismic hazard is one of the major topics for engineers since many existing reinforced concrete structures have been realized disregarding seismic design with minimal details with respect to present practice. In this context, seismic assessment is a primary issue in order to identify the best retrofitting solution with the aim to enhance the efficiency of existing buildings. In recent years, with the aim to enhance the seismic behaviour of reinforced concrete (RC) structures (with particular care to existing ones), the system of seismic isolation adopting friction pendulum (FPS) devices proved to be among the most diffuse and effective solution. The purpose of this paper is to explore the effectiveness of the refurbishment using FPS with single concavity devices on the performance of one irregular existing RC building placed into a highly seismic area of central Italy. First, the geometric and material characteristics of the building have been determined within the approach based on the "knowledge levels". Second, a suitable numerical model based on fiber-modelling approach have been established using SAP2000 including relevant mechanical non-linearities. Then, a set of 21 natural seismic inputs inclusive of 3 accelerations over vertical and horizontal directions have been adopted with the aim to perform non-linear (NL) dynamic simulations. The NL dynamic simulations have been performed considering the structural system both inclusive and not inclusive of the FPS isolator devices. The influence of actual distribution of infill masonry panels on the overall behavior of the structure has also been evaluated in both the mentioned above cases. Finally, the outcomes deriving from the NL dynamic simulations were helpful to assess the advantages of the intervention of retrofitting to improve the seismic performance of the building highlighting the influence of masonry infills.

Keywords: masonry infills; seismic protection; existing structures; performance analysis; RC buildings; irregular.

Citation: To be added by editorial staff during production.

Academic Editor: Firstname Lastname

Received: date
Accepted: date
Published: date

1. Introduction

The safety assessment of existing structures placed in areas with a relevant seismic hazard is one of the challenges for engineers over the last years [1-2]. In particular, during the 60's and 70's many buildings realized in reinforced concrete (RC) have been designed disregarding details in comparison to the current codes specifications for seismic areas [3-4]. In fact, the major part of such kind of buildings have been conceived for resistance mainly relating to gravity actions assuming a minor influence of horizontal ones (e.g., seismic events).

In this framework, the assessment for seismic actions is a crucial issue with the aim to identify proper dispositions to retrofit existing buildings [5-6] having particular care to under-designed structural systems [7]. In recent years, with the aim to enhance the seismic response of RC buildings, the system of seismic isolation adopting friction pendulum (FPS) devices proved to be among the most diffuse and effective solution [8-11]. Concerning the application to buildings constituted by RC structural frames, the major benefits relate to achieve a fundamental period not dependent on the mass of the structure placed up to the isolation level (i.e, superstructure). In particular, these devices allow significant energy dissipation capacity during the seismic motion by means of friction mechanism [12-13]. Moreover, with reference to the post-earthquake resilience, the self-recentering capability of the devices can permit fast recovery of building functionality [14]. For the mentioned above reasons, FP devices have been used in many situations in practice to isolate both buildings of new realization and existing ones [15-19]. In this framework, with the purpose to assess the compliance of the isolation system with respect to the reliability requirements of current design codes, the performance-based seismic design (PBSD) methodology can be adopted, as widely discussed by [12-13].

Contextually, the influence of the masonry infills on the response of RC framed structures have been widely investigated and recognized in its relevance on overall structural behaviour [20-22]. However, few studies have been devoted to understand their interaction with the adoption of seismic isolation systems as the FP devices [23-24] with particular reference to buildings characterized by significant irregularities (in plane, in elevation and related to the disposition and configuration of infills).

The purpose of this paper is to explore, in mono- and bi-variate probabilistic terms, the advantages of the refurbishment using FPS with single concavity devices of one irregular RC framed building placed in highly seismic area of central Italy investigating also the interaction between the masonry infills and the FP isolation system. After the identification of the material and geometric characteristics in line to the "knowledge levels" philosophy [3], a suitable numerical model based on fiber-modelling approach have been established in the SAP2000 software platform [25]. 3D non-linear dynamic analyses have been performed considering 21 natural ground motions [26-27] with the three accelerometric components to evaluate the performance of the RC building inclusive and not inclusive of the FP isolators. As mentioned above, the influence of the masonry infills on the seismic performance has been investigated [23-24]. In detail, the structure having base fixed to foundations (FB) and with isolation system (BI) has been analyzed with and without the presence of the masonry infills. The local influence due to the interaction between the RC frame and the both full and partial infill walls has been examined and accounted for during the definition of the numerical models. The outcomes of the 3D NL dynamic numerical simulations permit to assess the efficiency of the isolator devices to improve the seismic performance also of the RC framed building having both in plan and in elevation irregularities. As for engineering demand parameters (*EDPs*), the non-dimensional interstory drift (i.e., interstory drift index - *IDI*) and in plane displacement of the slider of the FPS with respect to the base of the device. The *EDPs* have been modelled through mono-variate and bi-variate lognormal distributions [12]. Finally, the exceedance probabilities for several values of the *EDPs* are computed and compared with respect to appropriate thresholds proposed by scientific literature [28].

2. Strategies to model behaviour of FPS and of masonry infills in RC framed structures

In this section the model herein adopted to reproduce the behavior of single-concave FP devices as well as the approach adopted to account for the influence of the masonry infills on seismic response of the RC framed structure are described.

2.1. Principles of behviour of FPS with single concavity

The FP isolators are devices able to improve the seismic performance of RC framed buildings in areas with a high seismicity [17, 19, 26]. Particularly, the FP devices allow to disconnect the superstructure from the foundation level and are able to accommodate most of seismic demand for displacement. In addition, these devices are able provide high energy dissipation by friction developed between the sliding surfaces [12]. These devices are realized through a slider device that can move on a surface having concave shape, which is characterized by a specific curvature radius *R* [30] and friction coefficient μ_d [31-32]. The adoption of single-concave FP leads to the main advantage of having the first natural period of the base isolated structure T_{is} dependent only on the curvature radius *R* [12]. The mentioned above dependence can be expressed as follows:

$$T_{is} = 2\pi\sqrt{R/g} \tag{1}$$

where the acceleation of gravity is denoted by g.

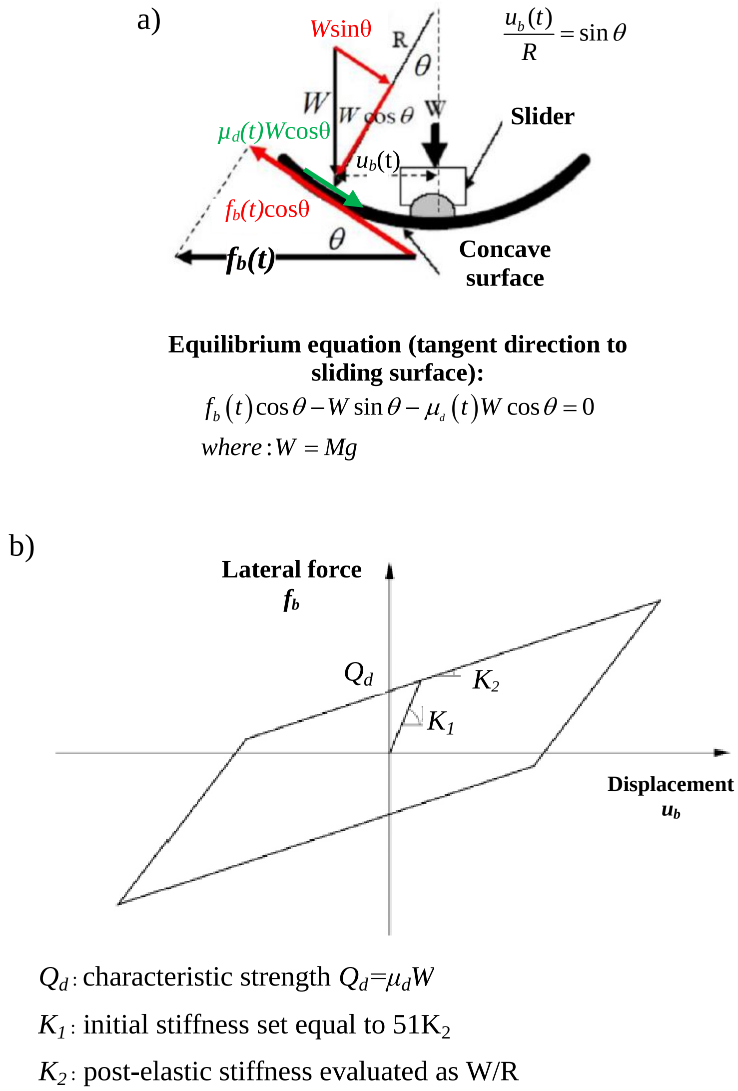

Figure 1. Representation of the free-body diagram of the FPS under imposed lateral force and related equilibrium equation to translation in horizontal direction of the slider (a) Theoretical non-linear hysteretic response of the FPS device (b).

The basic response in terms of dynamic equilibrium of the FPS device is represented in Figure 1(a) by means of the free-body diagram of the slider and related equilibrium equation with respect to translation along tangent direction to the sliding surface. After mathematical manipulation of the equilibrium equation showed in Figure 1(a) and assuming that the discrepancy between the normal direction to the sliding surface and the vertical one is negligible according to [11]-[12] (i.e., tangent direction to sliding surface coincides, reasonably, with the horizontal one), the restoring force $f_b(t)$ of the FP bearing device can be determined as follows:

$$f_b\left(t\right)=\frac{Mg}{R}u_b\left(t\right)+\mu_d\left(t\right)\mathrm{Mg}\,\mathrm{sgn}\left(\dot{u}_b\left(t\right)\right) \tag{2}$$

where M is the mass of the portion of structure pertaining the specific FPS device, $u_b(t)$ denotes the projection on the horizontal plane of the slider displacement relative to the ground, t is the time, $\mu_d(t)$ represents the coefficient of friction in dynamic regime, $sgn(\dot{u}_b(t))$ determine the sign of the velocity of the slider $\dot{u}_b(t)$during the motion.

Mechanical behavior of single-concave FPS devices may be idealized according to the non-linear hysteretic model proposed by [30], characterized by the definition of 3 parameters: the characteristic strength $Q_d = \mu_d W$ with W=Mg ; the stiffness after the elastic behaviour $K_2 = W/R$; the stiffness in elastic regime K_1, assumed equal to $51 \cdot K_2$. The representation of the theoretical hysteretic model for the FP device is reported in Figure 1(b). Regarding friction coefficient in dynamic regime, investigations of [31-32] suggest that $\mu_b(t)$ can be expressed as dependent on the sliding velocity $\dot{u}_b(t)$ as follows:

$$\mu_d\left(t\right)=\mu_{fast}-(\mu_{fast}-\mu_{slow})\exp(-\alpha\left|\dot{u}_b\left(t\right)\right|) \tag{3}$$

where the terms μ_{fast} and μ_{slow} represents the values of the coefficient of friction in regime of high and low, respectively, velocity of sliding $\dot{u}_b(t)$; α represent a constant that governs the variation of the coefficient of friction $\mu_b(t)$ between minimum and maximum values.

2.2. Modelling mechanical behaviour of masonry infills for seismic assessment

The principal role of infills in framed buildings derives from the need to confine the external environment from the internal one or to separate the internal compartments. As widely recognized, the masonry panels are able to interact with the surrounding RC structural frame in the presence of significant lateral actions [33]. This interaction produces both positive and negative effects on the overall response of the structure as can be deduced by the post-earthquake observed damage scenarios [34]. In fact, although the overall stiffness of the structural system turns out to be increased, the presence of infills leads to a reduction in the natural period with the related increase of the seismic spectral acceleration. Moreover, with particular reference to partially infilled panels, their presence provides additional stiffness locally increasing the shear demand on columns that can collapse with brittle mechanisms (e.g., captive and short column effects) [35]. For instance, despite the inevitable modeling issues, neglecting such elements in refined non-linear analysis of RC frames may not allow to properly estimate the actual stiffness, resistance and ductility of the structure system [33, 36-37]. The scientific literature proposes different approaches to account for masonry infills within the definition of numerical models of RC frames. These ones can be classified primarily in micro-modelling and macro-modelling [37].

In the present investigation the macro-modelling approach is adopted according to [37] for the fully infilled masonry panels to consider the effects deriving from the interaction between the infills and RC members. Specifically, they are reproduced by means of a single-strut model able to take into account the masonry mechanical non-linearities. According to [37], the strut can be defined adopting fiber-modelling approach with fibers characterized by the appropriate constitutive law able to reproduce the macro-behavior of the masonry panel [37]. As suggested in [37], the mentioned above constitutive law can be defined similarly to the one used for concrete, in which the peak strength f_{md0}, the corresponding deformation ε_{md0}, the ultimate resistance f_{mdu} and the related deformation ε_{mdu} are assigned depending on the mechanical and geometric properties of the masonry which are introduced in the next.

With reference to the macro-modelling of the partially infilled masonry panels, approaches able to take into account their non-linear behavior without large uncertainties are poor within the scientific literature. For instance, they have been reproduced by means of a single-strut model with elastic behavior in order to take into account unfavorable effects related on shear demand on columns [35]. In order to characterize the geometrical configuration of the macro-model with single strut, for each partial infill under examination, a micro-model using shell elements has been defined using SAP200 software platform [25] according to Figure 2. The thickness of the shell elements used for micro-modelling have been defined in accordance with the geometry of the masonry panel while, the interface between the shells and the surrounding RC frame has been reproduced using spring elements [25] able to take into account the friction between concrete and masonry (using a friction coefficient equal to 0.45 [37]).

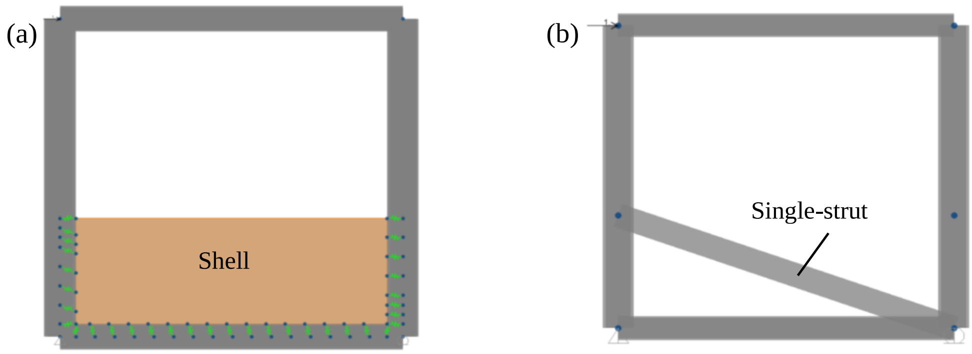

Figure 2. Micro-model with shell (a) and macro-model with single-strut (b) using SAP2000 for partially in-filled masonry panels.

In order to define an equivalent macro-model, the width of the single-strut was determined by a trial-and-error process until the same displacements, monitored at the top of the panel in presence of horizontal force, were obtained for the macro-models with respect to the micro ones. The mentioned above evaluation has been performed for all the different geometrical configurations of the partial infills of the RC frame. The elastic properties of material used for micro and macro-models have been determined according to the actual masonry mechanical characteristics as reported in the next sections.

Finally, concerning masonry panels with large openings, they were not included within the numerical model as their contribution to overall stiffness can be neglected.

The macro-models of the masonry panels so far established have been adopted within the numerical model of the existing RC framed structure with infills as commented in the following.

3. Analyzed irregular building and characterization of retrofitting intervention

In the present section, the description of the main features of the existing RC framed building are reported. Then, some geometrical aspects of the retrofitting intervention using single-concave FP isolators are also described.

3.1. Geometrical configuration of the structure

The existing RC framed building considered for the study is located in central Italy in a region with a very relevant seismicity. In particular, according to current Italian design code [3], the region is subjected to PGA (Peak - Ground - Acceleration) that is superior than 0.25g associated to exceedance probability of 10^{-1} in 50 years concerning life safety limit state. In the next, the main geometrical features of the building are reported focusing on the RC framed structure and masonry infills. The building has been realized during the '60s according to Italian design code that, at the time, was related to seismic design for small amount of specifications. For instance, the structure has been realized without appropriate seismic conception and detailing. The structure, built during the '60s, is constituted by a cast in situ RC structure that consists of orthogonal frames dislocated along *X* (i.e., longitudinal) and *Y* (i.e., transverse) directions. The foundations are stiff inverted continuous RC beams along the direction of the RC frames. The in-plan sizes of the building are 59.8 m in X direction and 12.2 m in *Y* direction. Figure 3 illustrates, schematically, the columns disposition with the related frames identified as *X1*, *X2* in the *X* direction and *Y1*, *Y2*, *Y3* along the *Y* direction.

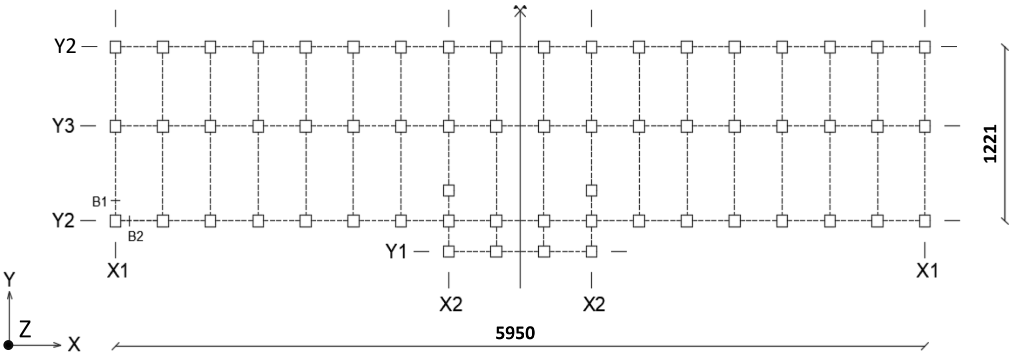

Figure 3. In-plan size of the RC building; characterization of the RC frames according to X and Y orthogonal directions [26]. Dimensions in centimeters.

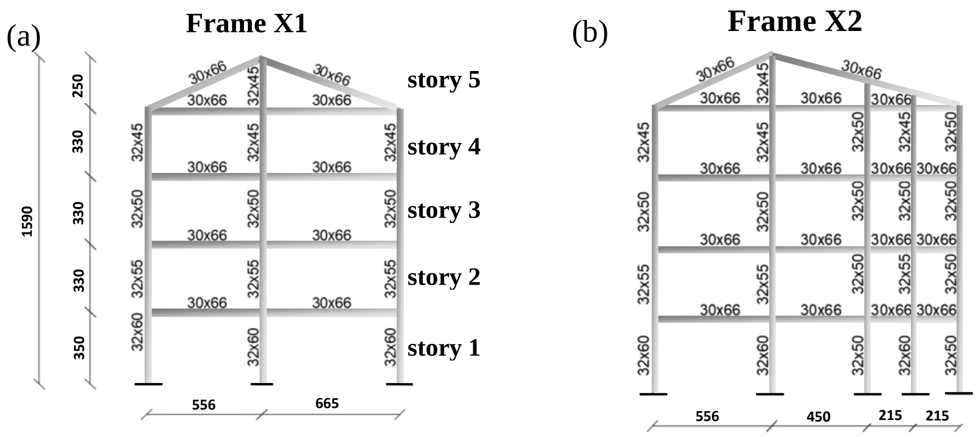

Figure 4. **D**etails of the RC frames that constitute the structure including cross-sections of main members in X direction [26]. Dimensions in centimeters.

With reference to the elevation, the maximum height of the building is equal to 15.9 m measured from the foundation level. The RC structure presents 5 stories including the roof level. The details of the geometry of the different RC frames that constitute the structure are reported in Figures 4 and 5. Concerning the boundary conditions, around the structure for a height of 3.5 m measured from the foundation level, there is a soil embankment that is able to limit displacements in X and Y directions of the story 1. This is a relevant aspect for the seismic behaviour of the structure and it is accounted for during the definition of the numerical model.

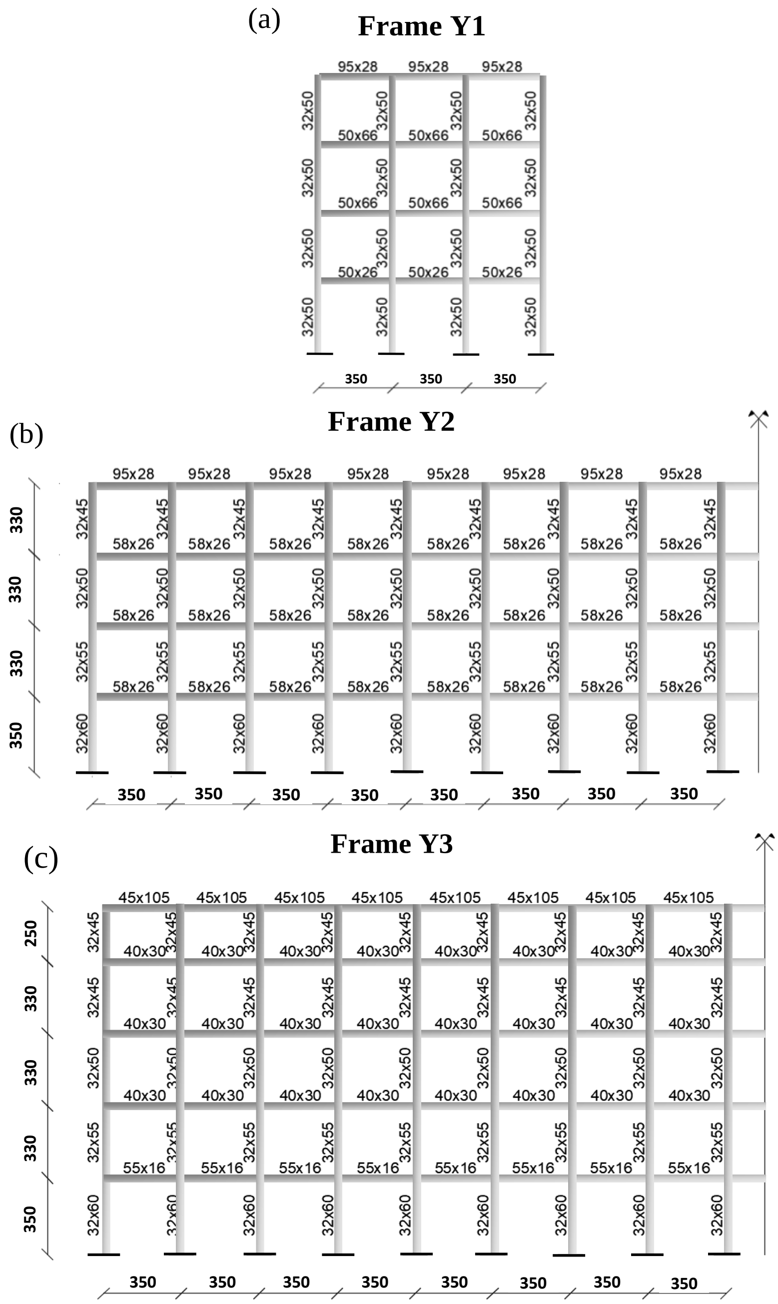

Figure 5. Details of the RC frames that constitute the structure including cross-sections of main members in direction Y [26]. Dimensions in centimeters.

Different types of members (i.e., columns and beams) are present as illustrated in Figure 6. The reinforcement arrangement (both for shear and bending) concerning each member is summarized in Table 1. Data from inspections denote that the clear concrete cover (in average) is equal to 3 cm for all structural members. The horizontal floors are built using lightened "latero-concrete" technical solution with RC joists and top slab. The RC joists are 16 cm height with a base of 10 cm with 0.5 m as center to center distance in transverse direction. They are oriented along the longitudinal direction (X), that is, according to the short beam floor pattern. The top slab is 4 cm thick and connect the joists realizing the floor and, for modelling purposes, it can be considered as able to realize a rigid floor able transfer horizontal actions to the longitudinal and transverse RC frames [3].

The only external masonry infills have been considered able to contribute to overall seismic response of the building. In particular, the masonry infills have a total thickness equal to 34 cm and are realized with the following stratigraphy: external facing in exposed brick (8 cm); air cavity (13 cm); internal facing in perforated bricks (12 cm) and internal cement plaster (1 cm). The disposition of the partially infilled and totally infilled masonry panel within the external RC frames of the structure is reported in Figure 7. It can be noted that the geometry of the external infills in the longitudinal direction is particularly unfavourable due to the presence of many partial infill panels.

Table 1. Shear and bending reinforcements for main members of the RC frames [26].

Type of structural member	Longitudinal reinforcement	Shear reinforcement (2 legs stirrups)	Longitudinal reinforcement	Shear reinforcement (2 legs stirrups)
Level (story)	**1**		**2**	
Column 1 Column 2	2ϕ20+5ϕ16 / 2ϕ20+5ϕ16	ϕ6@8mm	2ϕ20+5ϕ16 / 2ϕ20+5ϕ16	ϕ6@8mm
Column 3	2ϕ20+5ϕ14 / 2ϕ20+5ϕ14	ϕ6@12mm	2ϕ20+5ϕ14 / 2ϕ20+5ϕ14	ϕ6@12mm
Beam 1	*Beam midspan:* Sup. 2ϕ14 Inf. 5ϕ16	ϕ6@19mm	*Beam midspan:* Sup. 2ϕ14 Inf. 5ϕ16	ϕ6@19mm
	Beam ends: Sup. 2ϕ14 +5ϕ20 Inf. 2ϕ16	ϕ6@10mm	*Beam ends:* Sup. 2ϕ14 +5ϕ20 Inf.2ϕ16	ϕ6@10mm
Beam 2	*Beam midspan:* Sup. 2ϕ12 Inf. 5ϕ14	ϕ6@19mm	*Beam midspan:* Sup. 2ϕ12 Inf. 5ϕ14	ϕ6@19mm
	Beam ends: Sup. 2ϕ14 +5ϕ20 Inf. 3ϕ16	ϕ6@10mm	*Beam ends:* Sup. 2ϕ14 +5ϕ20 Inf. 3ϕ16	ϕ6@10mm
Beam 3	Sup. 2ϕ10 +2ϕ12 Inf. 2ϕ10 +2ϕ12	ϕ6@30mm	Sup. 4ϕ10 Inf. 2ϕ10 +2ϕ12	ϕ6@30mm
Beam 4	Sup. 4ϕ10 Inf. 4ϕ10	ϕ6@30mm	Sup. 4ϕ10 Inf. 4ϕ10	ϕ6@30mm
Beam 5	Sup. 4ϕ14 Inf. 4ϕ14	ϕ6@10mm	Sup. 4ϕ14 Inf. 4ϕ14	ϕ6@10mm
Level (story)	**3**		**4**	
Column 1 Column 2	2ϕ20+5ϕ14 / 2ϕ20+5ϕ14	ϕ6@10mm	2ϕ20+5ϕ14 / 2ϕ20+5ϕ14	ϕ6@12mm
Column 3		ϕ6@12mm		
Beam 1	*Beam midspan:* Sup. 2ϕ14 Inf. 5ϕ16	ϕ6@19mm	*Beam midspan:* Sup. 2ϕ14 Inf. 5ϕ16	ϕ6@19mm
	Beam end: Sup. 2ϕ14 +5ϕ20 Bottom 2ϕ16	ϕ6@10mm	*Beam end:* Sup. 2ϕ14 +5ϕ20 Bottom 2ϕ16	ϕ6@10mm
Beam 2	*Beam midspan:* Sup. 2ϕ12 Inf. 5ϕ14	ϕ6@19mm	*Beam midspan* Sup. 2ϕ12 Inf. 5ϕ14	ϕ6@19mm
	Beam end:	ϕ6@10mm	*Beam end:*	ϕ6@10mm

	Sup. 2ϕ14 +5ϕ20 Inf. 3ϕ16		Sup. 2ϕ14 +5ϕ20 Inf. 3ϕ16	
Beam 4	Sup. 4ϕ10 Inf. 4ϕ10	ϕ6@30mm	Sup. 4ϕ10 Inf. 4ϕ10	ϕ6@30mm
Beam 5	Sup. 4ϕ14 Inf. 4ϕ14	ϕ6@10mm	Sup. 4ϕ10+ 1ϕ12 Inf. 2ϕ10+ 1ϕ12	ϕ6@10mm
Level (story)		**5 (Roof)**		
Beam 6	Sup. 2ϕ16 + 5ϕ20 Inf. 3ϕ16 + 2ϕ14	ϕ6@10mm	-	-
Beam 7	Sup. 4ϕ10 Inf. 2ϕ12 + 2ϕ10	ϕ6@10mm	-	-

The adoption of FPS devices for the here described refurbishment has been exploited by means the introduction of a disjunction between foundation level and superstructure in correspondence of the columns of the story 1, as shown in Figure 8. In detail, the columns at the base of the story 1 can be cut and, thanks the use of temporary supports, the FP devices can be installed. Moreover, the tops of the columns at the level of the substructure (i.e., below the isolator devices) have been connected by RC beams to enhance the robust response of the structure equipped by FPS against potential malfunction of one or more of the devices [5]. More details about the isolation system design are given in next sections.

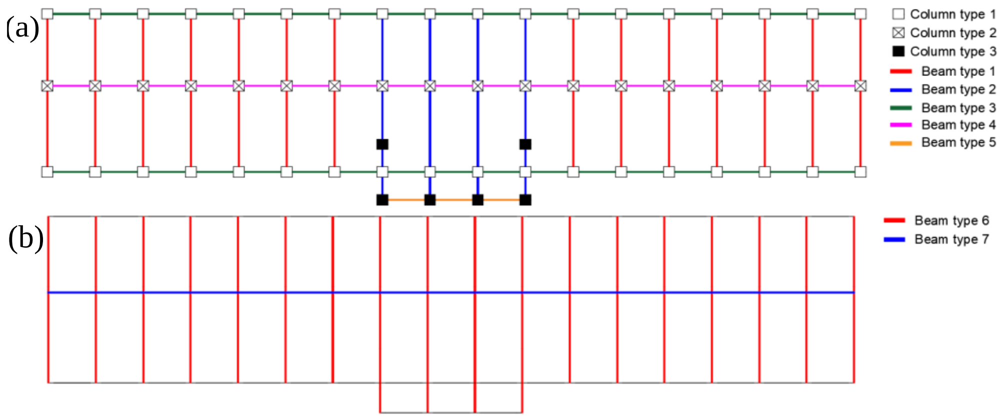

Figure 6. Characterization of beams and columns within the RC structure [26]: (a) typical story; (b) roof.

Figure 7. Identification of external totally and partially masonry infilled frames. Frontal and lateral views of the building (a); Back and lateral views of the building (b).

Figure 8. Position of the isolation level (red dashed line) with location of the single-concave FP devices.

3.2. Characterization of material properties of the RC structure and masonry panels

The determination of the materials mechanical characteristics has been performed by means of destructive and non-destructive tests. With reference to the "knowledge levels" (KL) approach [3], the achieved level of knowledge was compatible with the third one (i.e., KL3). For instance, the confidence factor [3] for material properties can be adopted as equal to 1.00. Then, the material properties used for the non-linear numerical analyses and structural verifications will be equal to the mean ones (i.e., experimental) for concrete, reinforcement and masonry. The mean values of material properties have been determined according to statistical analysis of tests results. In detail, the cylinder concrete compressive strength (mean value) f_{cm} has been determined by means destructive test of cores drilled from several structural elements. Its value, after statistical treatment of the data, has been estimated as 25.2 MPa. On few sampled concrete cores, measurements of axial strain levels have been conducted with the aim to quantify the value of secant elastic modulus E_{cm} (mean value). The value of E_{cm} turns out to be equal to 22000 MPa.

As for the steel reinforcement bars (FeB38k), the related characteristics have been estimated by means of tensile tests on specimen of reinforcing bars taken from different structural components. The mean value of tensile yielding f_{ym} strength turned out to be equal to 374 MPa.

In addition, tests on masonries were carried out to determine the mechanical parameters, such as elastic modulus $E_{m1,2}$ (in horizontal and vertical directions, respectively) and shear strength f_{vm} by diagonal compression tests. The vertical compressive strength f_{m2} was instead inferred through the use of Italian standard [3] depending on the masonry panel stratigraphy. The horizontal compressive strength f_{m1} has been considered equal to the 50% of f_{m2} [3]. All the mentioned above parameters should be considered as mean values and are summarized in Table 2. These values are adopted according to the methods for macro-modelling introduced in Section 2.2 with the aim to reproduce the influence on structural behaviour of masonry infills.

Table 2. Mechanical properties of masonry panels.

E_{m1} [MPa]	E_{m2} [MPa]	f_{vm} [MPa]	f_{m1} [MPa]	f_{m2} [MPa]
4325	4804	0.75	3.9	7.8

4. Non-linear numerical modelling and structural analysis

In the next, the assumptions adopted to define the numerical models [25] and to perform the NL dynamic simulations of the investigated RC building are listed in agreement with [26], [39-40] also with reference to the characterization of ground motion inputs.

4.1. Definition of the NL numerical models related to RC framed building including infills for base-fixed and base-isolated structure

The RC framed building under investigation have been numerically reproduced in line to the geometrical and materials characteristics introduced in the previous sections using SAP2000 [25]. As for the modelling of the RC columns, it has been performed with the assumption of full restraint at the level of the rigid inverted RC beams that constitutes the foundations of the building. Furthermore, the behaviour of the stiff fields of "latero-cement" floors have been reproduced by appropriate membrane constraints in SAP2000 [25]. As introduced in previous sections, the building, up to the level of the story ,1 is surrounded by an embankment of soil. The presence of the latter has been included within the numerical representation of the structures accounting for its restraining effect for in plane (i.e., X and Y directions) displacements of the story 1 [26].

Concerning the modelling of the main structural elements, characterized by RC columns and RC beams, it has been adopted a discretization approach based on fiber cross-section with the aim to define the non-linear behavior of the plastic hinges according to concentrated plasticity philosophy (SAP2000 [25]). Specifically, for each type of cross-section, the constitutive laws of the fibers have been distinguished between steel longitudinal reinforcement, core (i.e., confined by stirrups) and cover concrete. The plastic hinges based on fiber discretization allow to take into account the axial load and bending (biaxial) inter-relationship [25]. The non-linear response of the hinges takes place within a predetermined length L_p that denotes the plastic hinge length [44]. The plastic hinge length L_p has been determined in line to the equation proposed by [45].

The constitutive law of [41] has been adopted to simulate non-linear response in compressions of fibers representing the core and the cover concrete. The related tensile behavior has been modelled by means LTS (i.e., Linear Tension Softening). All the needed mechanical characteristics of concrete have been obtained as a function of the mean value of the experimental results for cylinder strength in compression f_{cm} and modulus of elasticity E_{cm} in line to the specifications of EN1992 [43]. With the aim to take into account the degradation of the mechanical properties due to the accumulation of damage during the seismic event, the model of [46] has been adopted.

With refence to the constitutive law for bars reinforcement, an elastic with perfect plasticity model has been used, having care to limit the ultimate strain at the value of 7.5% [43]. According to the experimental tests, the mean value f_{ym} has been adopted as yielding strength concerning both the compressive and tensile behavior. The modulus of elasticity has been set to the value of 200000 MPa.

As anticipated in Section 2, the masonry infills have been modelled adopting a macro-modelling approach. The partially infilled panels have been modelled using "frame elements" in SAP2000 [25] active in compression only with elastic behavior. The geometric average elastic modulus of masonry between E_{m1} and E_{m2} has been adopted. The fully infilled frames have been modelled adopting link element "Multilinear plastic" [25] active in compression only. The related force-displacement non-linear constitutive law has been derived according to [37] as explained in Section 2. The weight (and related mass) of the masonry infills have been considered within the numerical analyses as an additional permanent action on the RC frames.

As for modelling of FPS devices for the base isolated building, the link element with non-linear behavior denoted as "Friction Pendulum" have been adopted according to SAP2000 [25] library. The non-linear mechanical response of the links for what concerns the in plane displacements along X and Y degrees of freedom (i.e., DOFs) has been defined according to the parameters affecting the FPS behavior as explained in Section 2 (i.e., R, K_1, K_2 and $\boldsymbol{\mu_d(t)}$). The vertical displacement DOF of the link representing the FPS it has been modelled with linear elastic behavior active in compression only.

The selection of the appropriate value of R is related to the achievement of a specific isolation period T_{is} of the building in line to the Eq.(1). In line to Section 2, the stiffnesses K_2 and K_1 have been determined as a function of the axial load on the specific FPS isolator device. The friction coefficient in dynamic regime as a function of time has been modelled in SAP2000[25] according to [31] and [32]. The related value has been determined in the function of the axial load applied on each device with reference to the empirical approach of [31]. The summary of the properties associated to the different FPS isolators are reported in Table 3 together with their disposition in plan as showed by Figure 9. As reported in Figure 10, four different numerical models have been realized differentiating between the fixed-base/base-isolated structure without masonry infills and fixed-base/base-isolated structure with masonry infills.

Table 3. Properties of FPS devices in the function of the axial load.

Type	*FPS 1*	*FPS 2*	*FPS 3*	*FPS 4*	*FPS 5*	*FPS 6*	*FPS 7*	*FPS 8*	*FPS 9*
R [m]					1.5				
K_2 [kN/m]	355	442	471	293	413	400	431	335	382
K_1 [kN/m]	18080	22517	23996	14957	21038	20381	21958	17093	19460
μ_{Slow} [%]					1				
μ_{Fast} [%]					3				
α [s/m]					30				

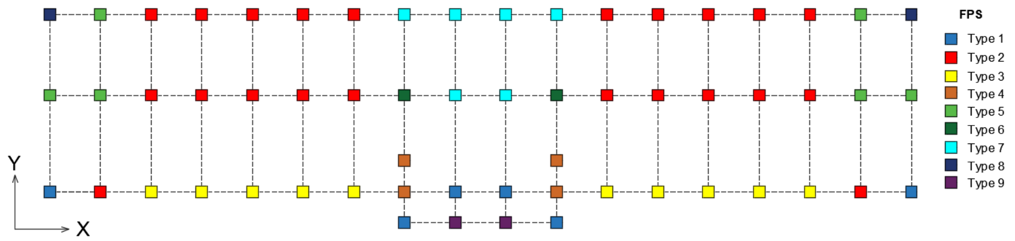

Figure 9. In plan location of the single-concave FPS devices with different modelling characteristics [26].

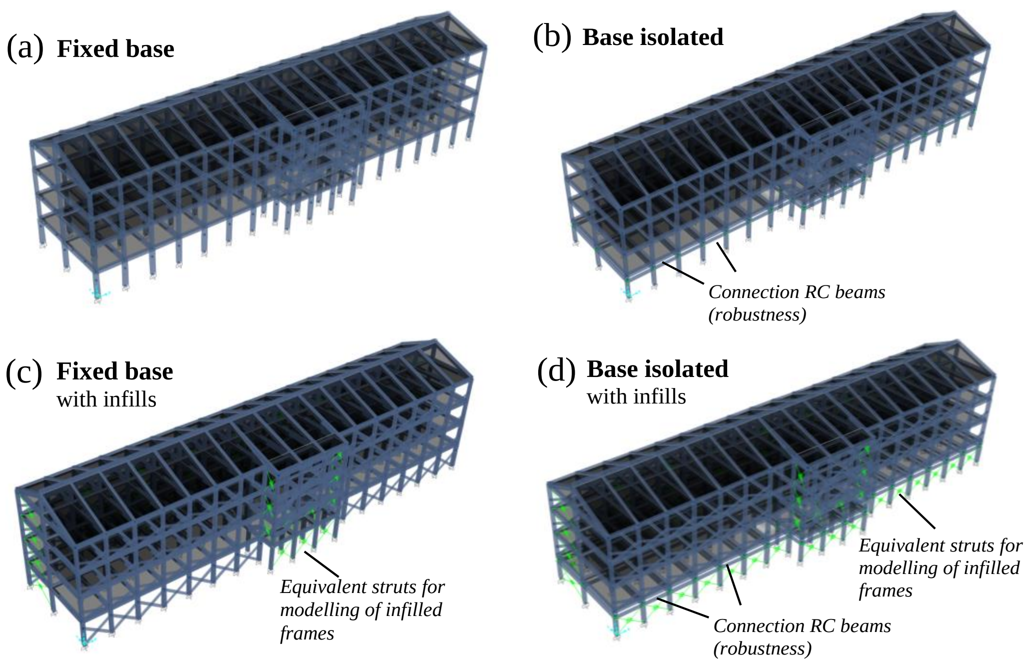

Figure 10. NL numerical idealization for fixed-base (a) and base-isolated (b) structures without infills and fixed-base (c) and base-isolated (d) structures with infills using SAP 2000.

4.2. Definition of the sesimic inputs and related demand

The seismic demand has been determined adopting as Intensity Measure (IM) the value of the pseudo-acceleration S_a in elastic regime. The site related response spectrum associated to 50 years as reference period for limit state of life safety have been adopted in line to [3]. The values of the damping coefficient ξ have been distinguished between the fixed-base and base-isolated structure adopting 5% for the former and 2% for the latter one [12]. Figure 11 shows the adopted elastic response spectra.

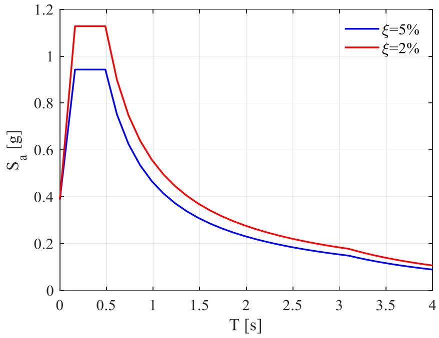

Figure 11. Adopted response spectra in elastic regime according to limit state of life safety [3] and [26].

The set of ground motion inputs to realize the NL dynamic simulations are constituted by 21 natural records composed by 3 acceleration components along the in plane and vertical directions as used in [12] and furtherly in [26]. In [12], the selection of the 21 inputs has been performed from the ESM (European - Strong - Motion database) [27].

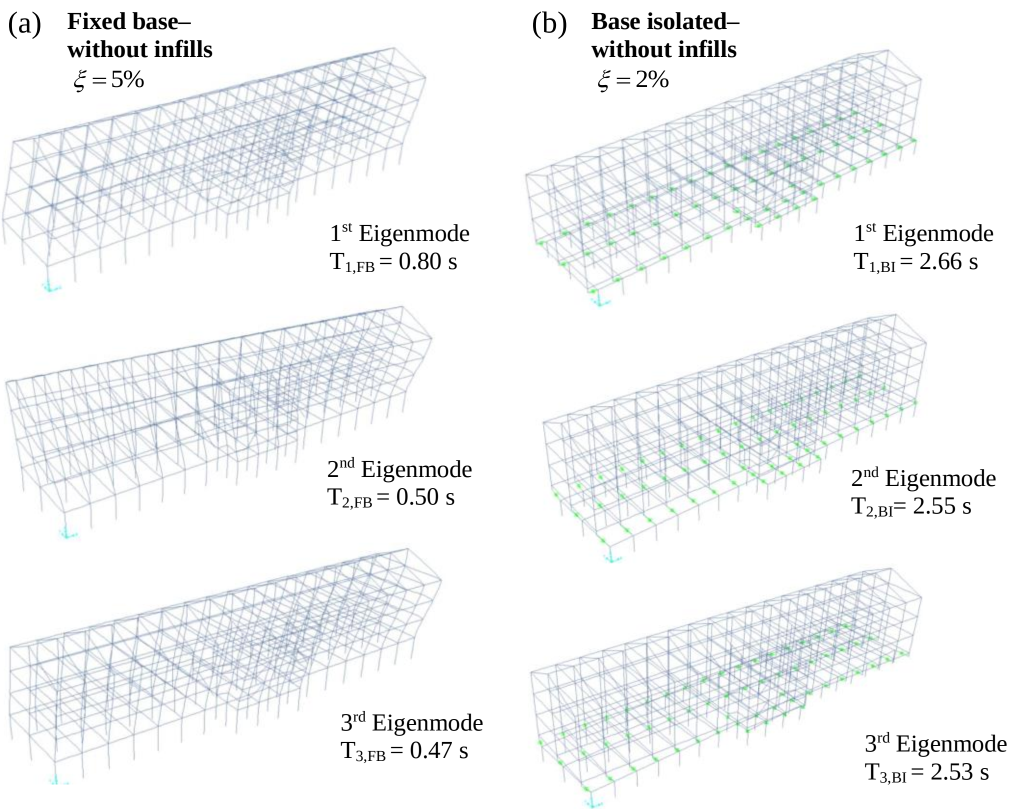

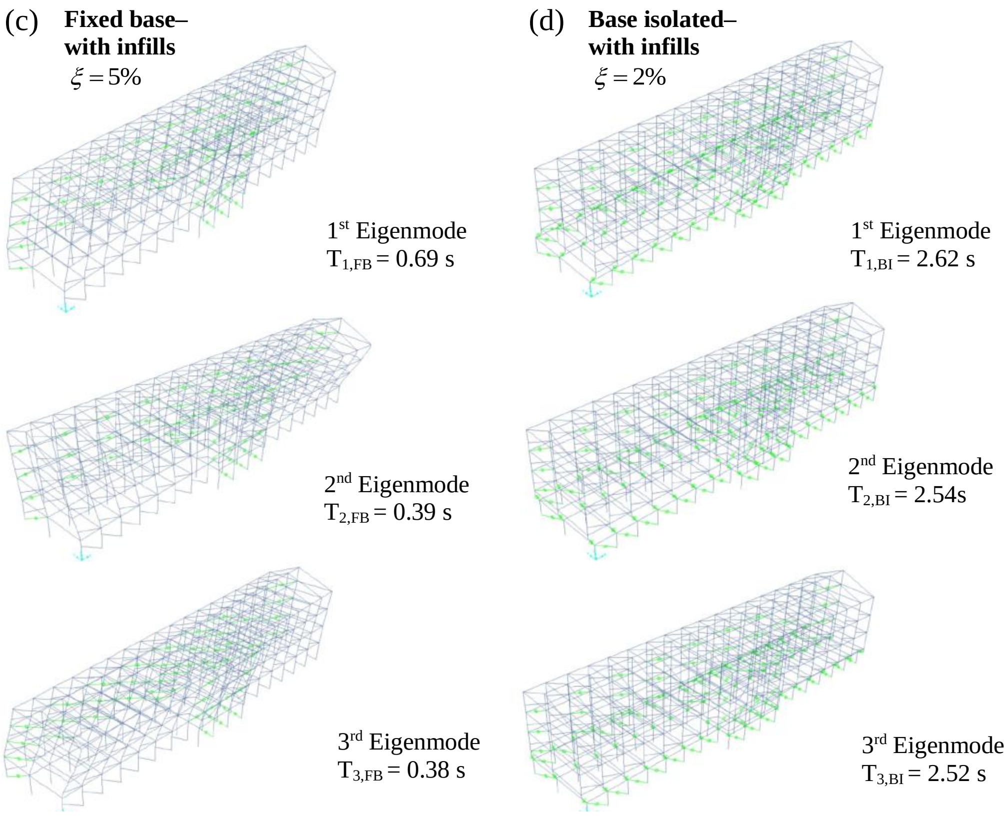

Figure 12. Representation of the first three eigenmodes for the fixed-base structure with (a) and without infills (c) and for the base-isolated structure with (b) and without infills (d).

The structural response of both fixed-base and base-isolated buildings have been investigated by means of modal analysis. Figure 12 reports the summary of the first three eigenmodes (and related periods of vibration) associated to the different structural configurations including the influence of the infills. It can be highlighted that no significant variations in the modal shapes occur due to the presence of infills for both fixed-base and base-isolated structures. In case of fixed-base structure, as expected, the presence of the infills reduces significantly the periods of vibration due to their stiffening effects. On the opposite, the periods of vibration of the base isolated structures are not strongly affected by the infills.

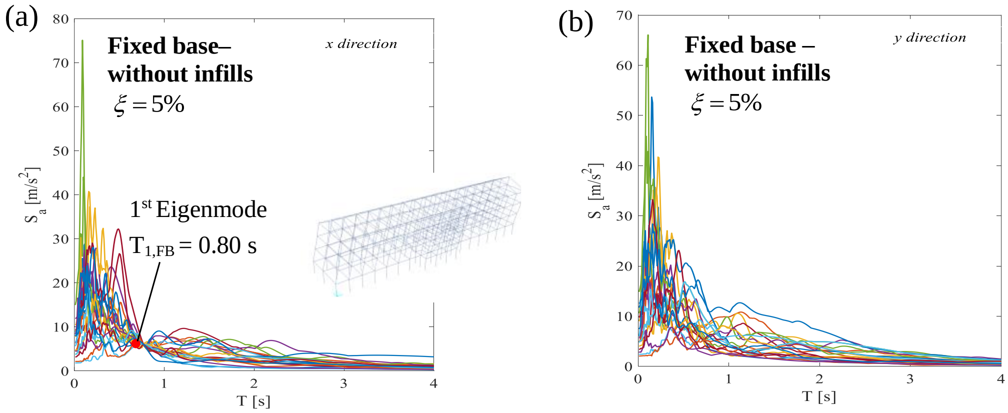

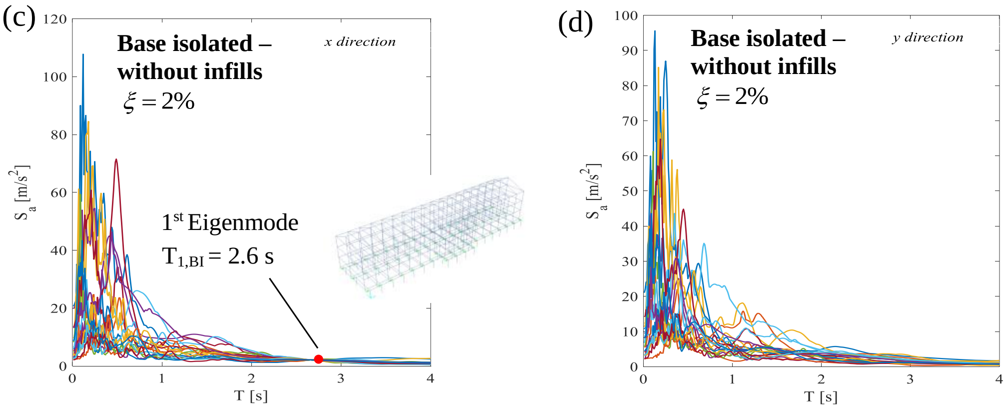

Figure 13. Scaled spectra of pseudo-acceleration for fixed-base (a)-(b) and base-isolated (c)-(d) building related to natural seismic inputs along *X* (a)-(c) and *Y* (b)-(d) directions. Numerical models without infills.

With the aim to ensure spectrum compatibility with the spectra presented in Figure 11, each record have been properly scaled for what concern the X direction component. In particular, the IM evaluated in concomitance of the fundamental period T_1 of the structure related to the elastic spectrum of the specific record have been scaled to the IM of the design spectra of Figure 11. This operation has been performed for both fixed-base and base-isolated structures including and not including the effect of infills made of masonry. The response spectra related to the selected natural records and associated to the different structural configurations are showed in the Figure 13 and Figure 14. Note that for the base isolated infilled frame the scaled records are almost equal to the ones corresponding to the base isolated bare frame (i.e., without account for the infills). This demonstrates the minor influence of the presence of infills in modification of the natural frequency of the base isolated building. In general, the presence of the infills reduce from 0.80s to 0.69s the natural frequency of the fixed-base building.

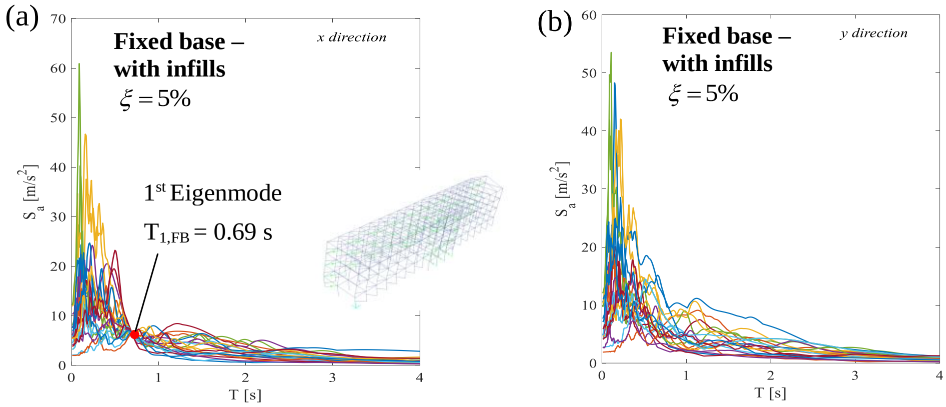

Figure 14. Scaled spectra of pseudo-acceleration for fixed-base (a)-(b) building related to natural seismic inputs along *X* (a) and *Y* (b) directions. Numerical models with infills.

4.3. Execution of the NL dynamic numerical simulations for investigated building

The set of non-linear equations of motion under seismic input related to the analyzed building have been solved by means of the method of direct integration in line to [49-50]. Both geometric and mechanical non-linearities have been included within the analyses. As the modelling approach based of fiber plastic hinges, as already described, does not account for the possible shear failure before the development of cross-section plasticity resources, specific shear verification has been performed according to EN1992 [43] for each step of the dynamic non-linear simulations.

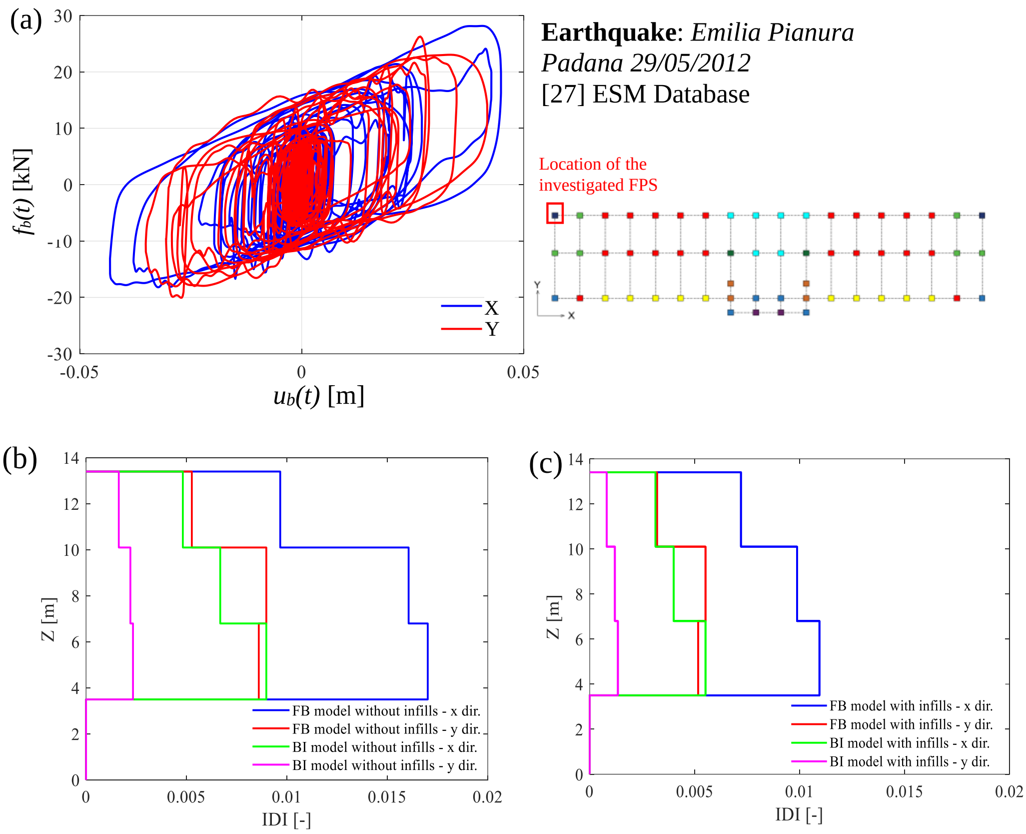

Figure 15. Response of one of the FP devices under seismic excitation (a); parallelism related to mean value of the *IDIs* achieved for different stories for numerical models of fixed-base and base-isolated building without (b) and with (c) masonry infills.

With particular reference to the comparison between the fixed-base and base-isolated building, the presence of the FPS devices allows to prevent the shear failure in columns where partial infills are located with significant reduction of the short column effect.

The outcome of the NL dynamic simulations has been quantified in terms of peak value of the inter-story drift index (*IDI*) for each story of the building for what concerns the in-plane directions (i.e., X, Y). In Figure 15(a), the response of the corner FP device (that turns out to be the most critical one) to the seismic excitation associated to one of the scaled seismic inputs (i.e., earthquake of "Emilia Pianura Padana 29/05/2012") [27] (that corresponds to the EQ5 with reference to the database reported by [26]) is reported to demonstrate its agreement with the theoretical model of Figure 1(b). In the force-displacement graph of Figure 15(a) the irregularity of hysteresis cycles is due both to the variability of the dynamic coefficient of friction with the sliding velocity and to the effects induced by the vertical accelerometric component of the seismic record. Moreover, in Figure 15(b)-(c), the IDIs, computed as average values between all the seismic records, are reported in the function of the building height from the foundation level for each numerical model herein considered. It can be recognized that the IDIs along Y axis are smaller if compared to the ones along X due to the different stiffness of the frames oriented in Y and X directions, respectively. The results show a significant reduction of the IDIs in presence of the isolation system demonstrating its usefulness also for the case of irregular buildings. Comparing Figure 15(b)-(c), it can be appreciated the increase of stiffness due to the presence of masonry infills.

5. Analysis of structural performance by probability-based approach

Starting from the outcomes of the 3D NL dynamic simulations, the horizontal relative displacements of the isolators d_{FPS} and the *IDIs* have been the starting point to analyze the structural performance of both fixed-base and base-isolated systems in probabilistic terms. In particular, it has been assumed that both d_{FPS} and *IDIs* are lognormally distributed [12], with mean value μ and standard deviation σ. By performing a statistical inference analysis, the hypothesis of lognormal distribution has passed the test with significance level of 5%. The parameters of the probabilistic distribution have been computed adopting the Maximum Likelihood method according to [51].

Table 4. Limit states thresholds in terms of IDI (FB and BI structure) [12],[28].

Limit state	IDI [%] for FB structure	IDI [%] for BI structure	P_f in 50 years [-]	P_f in 1 year [-]
Fully operational limit state LS1	0.50	0.33	5.0×10^{-1}	1.4×10^{-2}
Operational limit state LS2	1.00	0.67	1.6×10^{-1}	3.5×10^{-3}
Life safety limit state LS3	1.50	1.00	2.2×10^{-2}	4.5×10^{-4}
Near-Collapse limit state LS4	2.00	1.33	1.5×10^{-3}	3.0×10^{-5}

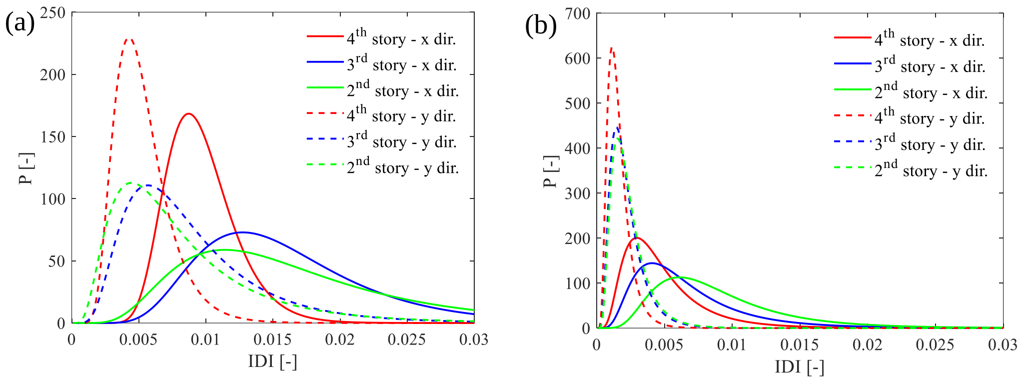

Figure 16 Mono-variate log-normal distribution (PDFs) related to the *IDIs* oriented in *X* and *Y* direction: fixed-base model (a), base-isolated model (b); (without masonry infills) [26].

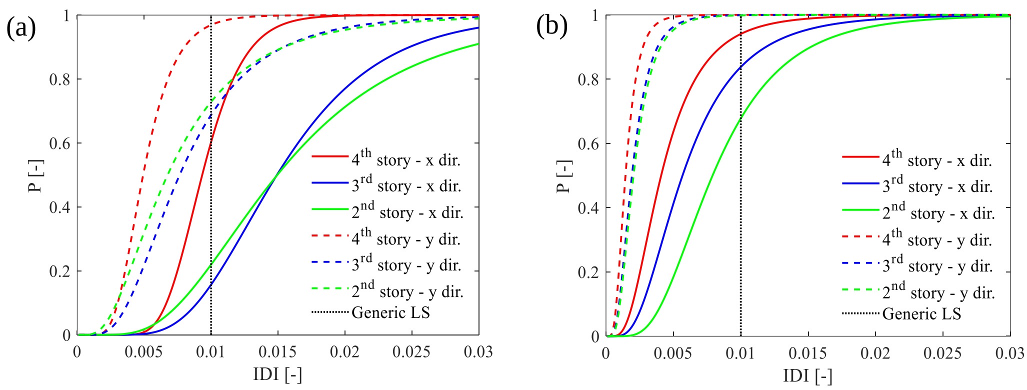

Figure 17. Mono-variate log-normal distribution (CDFs) related to the *IDIs* oriented in *X* and *Y* direction: fixed-base model (a), base-isolated model (b); (without masonry infills) [26].

In Figures 16-17 it is illustrated the mono-variate lognormal distributions, by presenting either the results in terms of probability density functions (PDFs) and cumulative density functions (CDFs), and by making a comparison between the fixed-base and base-isolated structure, each of one considering once the absence of the masonry infills and once including those elements. Table 4 reports the limit state (LS) thresholds according to [28] in terms of IDI for both the structural systems (i.e., fixed-base and base-isolated) associated to an acceptable limit for probability of exceedance in 50 years and 1 year.

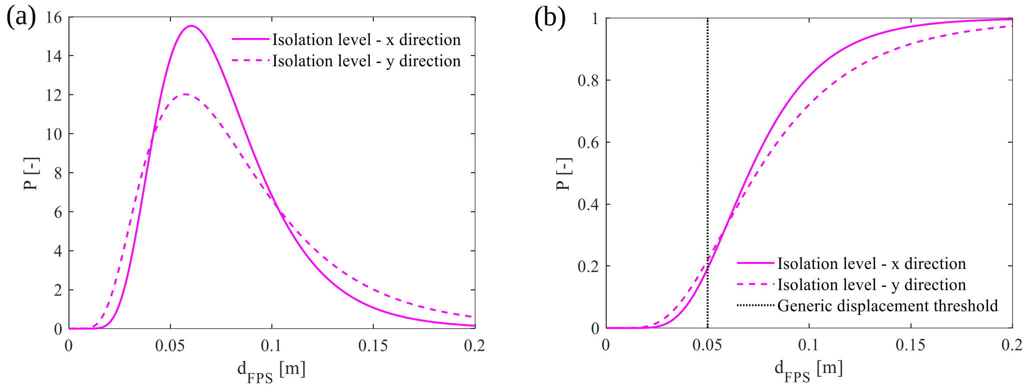

Figure 18. Mono-variate log-normal distribution (PDFs (a) and CDFs (b)) related to the in plane relative displacement with respect to the ground of the isolation level oriented in *X* and *Y* direction (without masonry infills) [26].

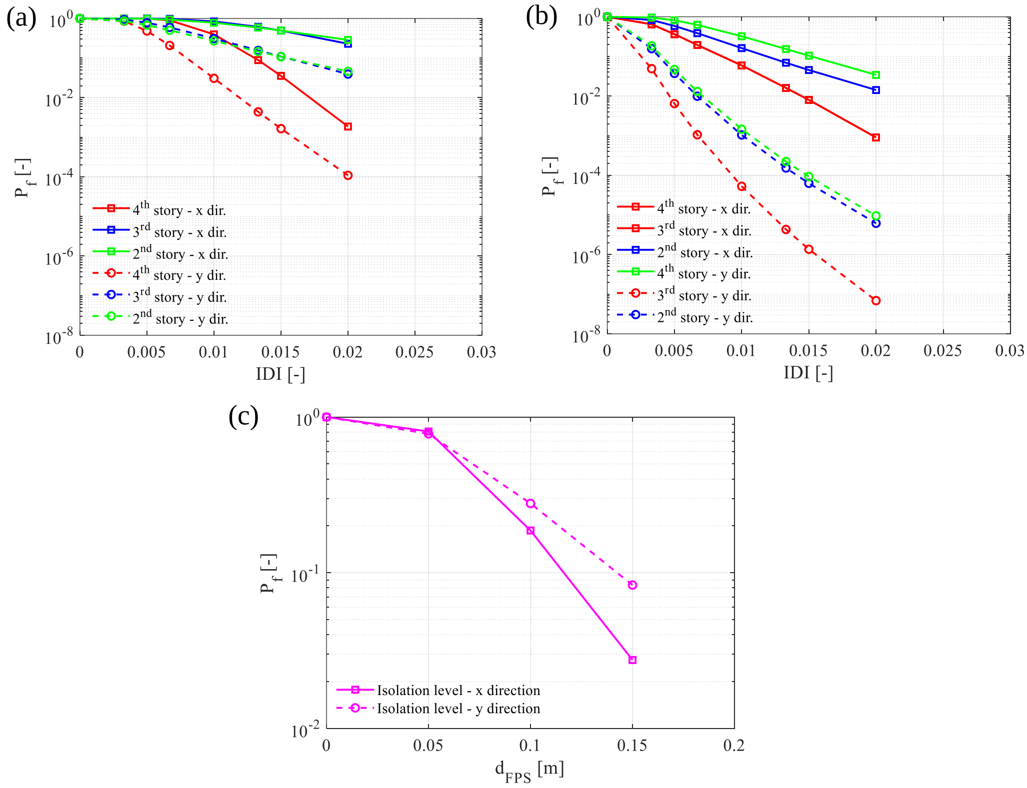

Figure 19. Probabilities of exceedance with mono-variate assumption in logarithmic scale: base fixed model (a); base isolated model (b); Isolator devices for base isolated model (c); (without masonry infills) [26].

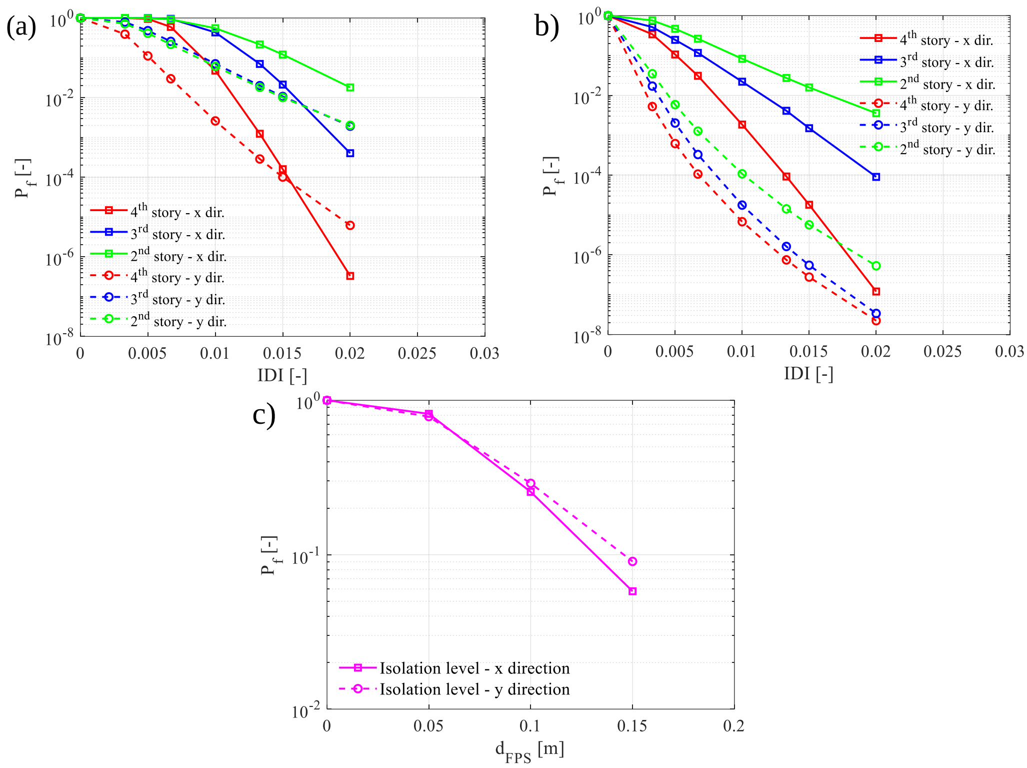

Figure 20. Probabilities of exceedance with mono-variate assumption in logarithmic scale: base fixed model (a); base isolated model (b); Isolator devices for base isolated model (c); (with masonry infills).

Figure 16(a-b) reports for both fixed-base and base-isolated buildings (without masonry infills), the mono-variate lognormal probability distribution functions obtained from the *IDIs* and considering different stories, while, Figure 17(a-b) reports the related cumulative distribution functions.

In particular, Figure 17(a-b) illustrates, respectively, the mono-variate lognormal probabilistic and cumulative distribution functions of the d_{FPS} including both the *X* and *Y* directions, for the base isolated building (without masonry infills). First of all, it is shown that the horizontal displacement and the interstory drift index in the X directions is considerably larger than in the other direction, being less stiff in that direction. In addition, it is demonstrated that the retrofit allows a reduction in terms of probability of exceedance P_f of the defined limit state. The exceedance probabilities for the isolation level and for both the fixed-base and base-isolated buildings (without masonry infills and considering the different stories) are shown in Figure 18(a-c). It is shown that the isolation technique is able to decrease the *IDIs* and, thus, to significantly reduce the probability of exceedance if compared to the non-isolated structure.

The previous conclusion is generally true with and without considering the presence of masonry infills as show in the Figure 20. As for the effects of the masonry infills, it can be highlighted as they affect the order of magnitude of the *IDIs* as well as the related exceeding probabilities.

Furthermore, the tri-dimensional response of either the fixed-base structure and the base-isolated one can be performed evaluating the degree of correlation between the abovementioned parameters *IDIs* and d_{FPS} along the two directions *X* and *Y* of the planar scheme of the structure. Then, the joint log-normal distributions have been computed according to [12].

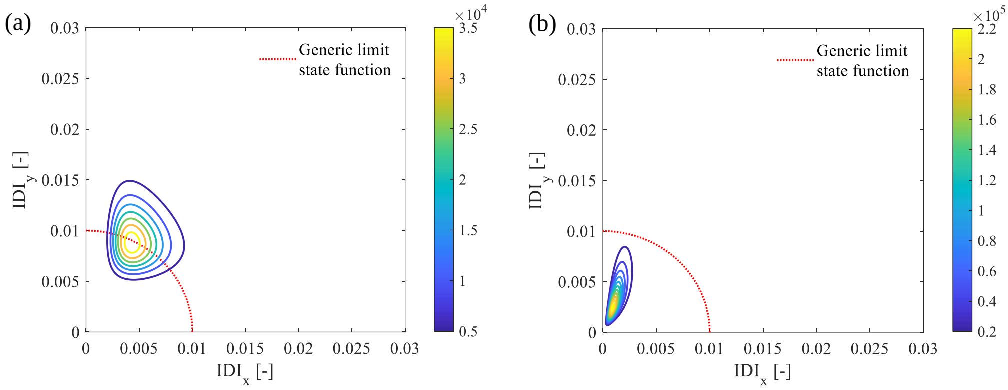

Figure 21. Level curves of the joint PDF for the 4th storey with a generic limit state: fixed-base model (a); base-isolated model (b); (without masonry infills).

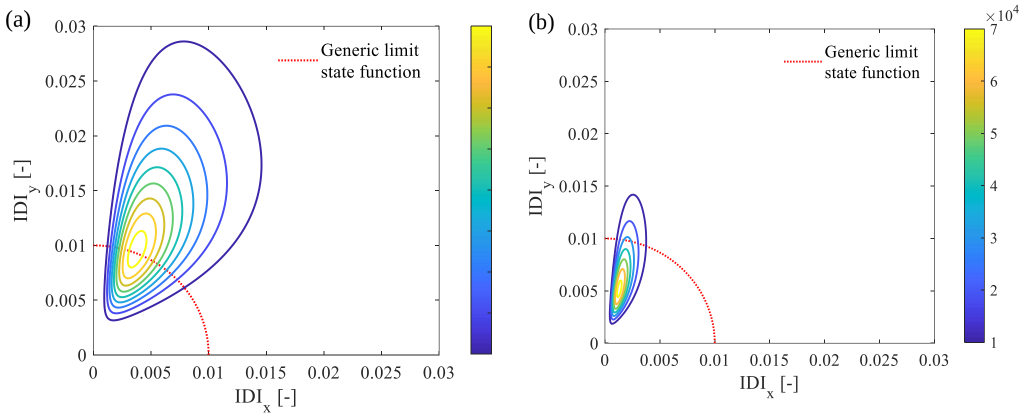

Figure 22. Level curves of the joint PDF for the 2nd storey with a generic limit state: fixed-base model (a); base-isolated model (b) (without masonry infills).

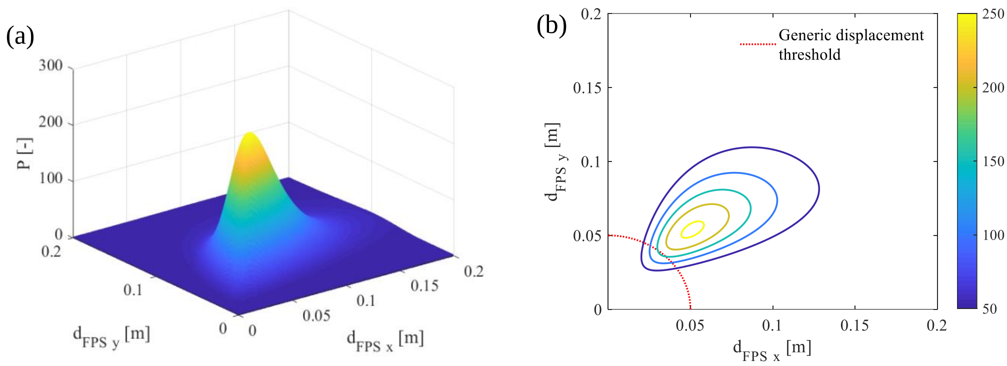

Figure 23. 3D view of the Joint PDF for the isolation storey (a) and level curves (b) with a generic displacement threshold (without masonry infills).

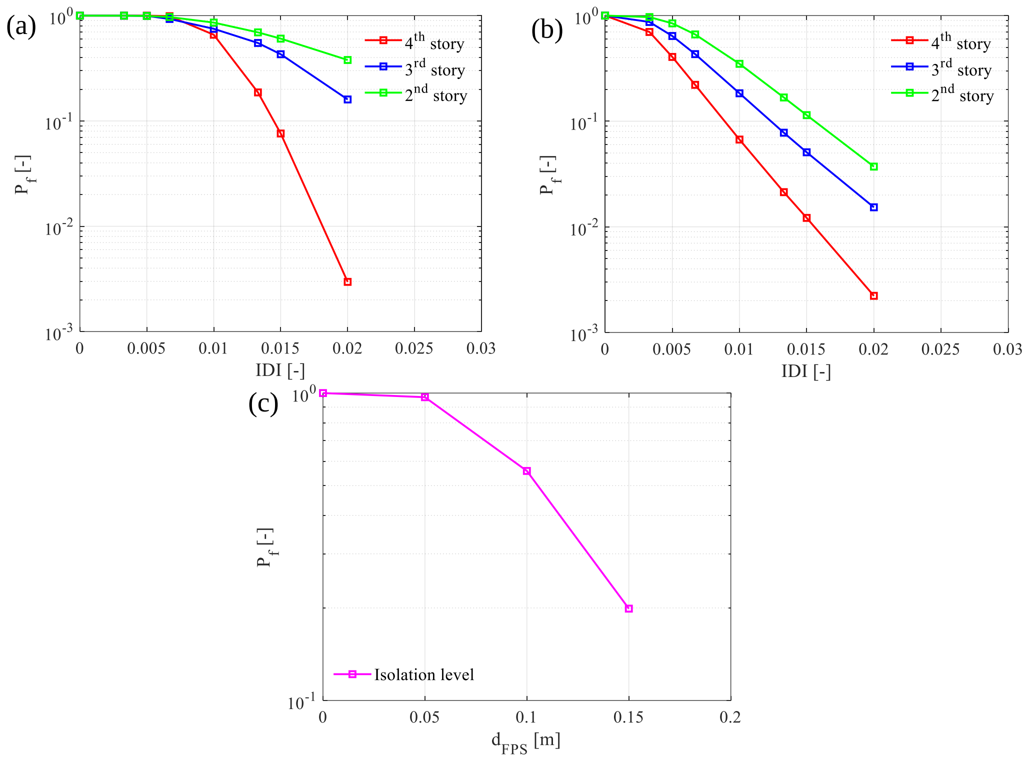

Figure 24. Probabilities of exceedance with bi-variate log-normal assumption in logarithmic scale: base fixed model (a); base isolated model (b); Isolator devices for base isolated model (c); (without masonry infills).

As far as the probability of failure in the case of jointly distributed variables is concerned, it must be calculated by integrating the generic JPDF, $f_{Z_X Z_Y}(Z_X, Z_Y)$, where Z_X denotes IDI_x or d_{FPSx} whereas Z_Y denotes IDI_Y or $d_{FPS,Y}$. Figures 21-28 illustrate mainly the level curves of the Joint PDFs, together with a certain limit state area, considering the cases with and without masonry infills and for both fixed-based and base-isolated buildings. As examples, regarding the superstructure only results related to the 4th storey and the 2nd storey are presented.

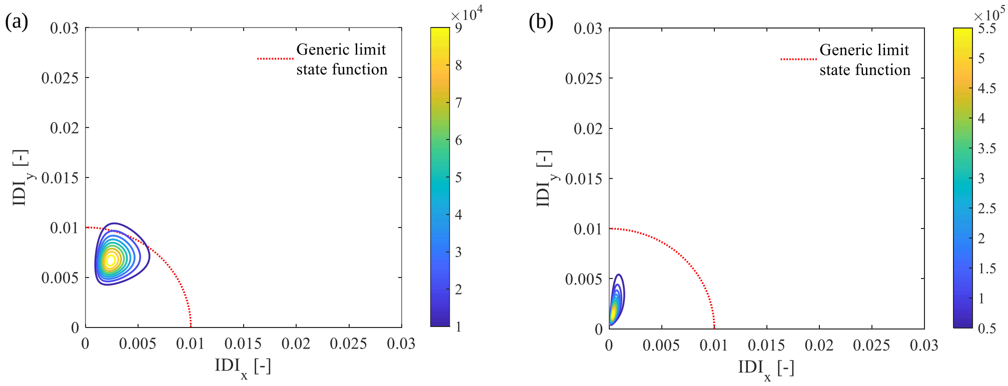

Figure 25. Level curves of the joint PDF for the 4th storey with a generic limit state: fixed-base model (a); base-isolated model (b) (with masonry infills).

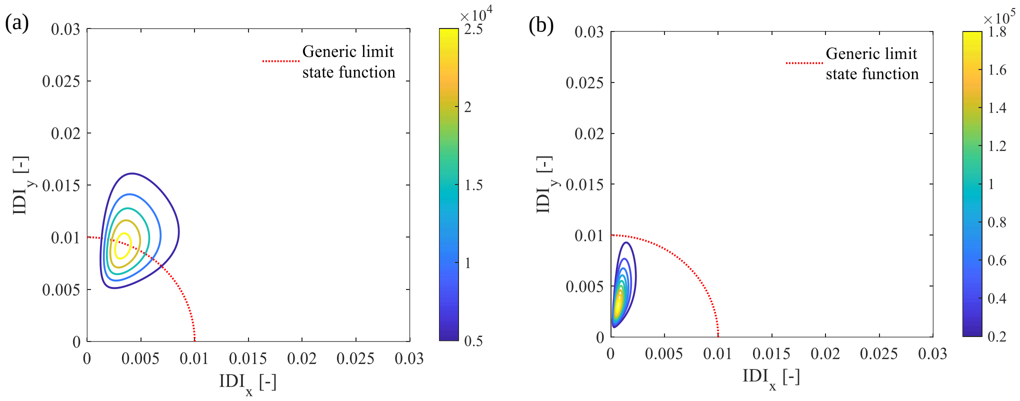

Figure 26. Level curves of the joint PDF for the 2nd storey with a generic limit state: fixed-base model (a); base-isolated model (b); (with masonry infills).

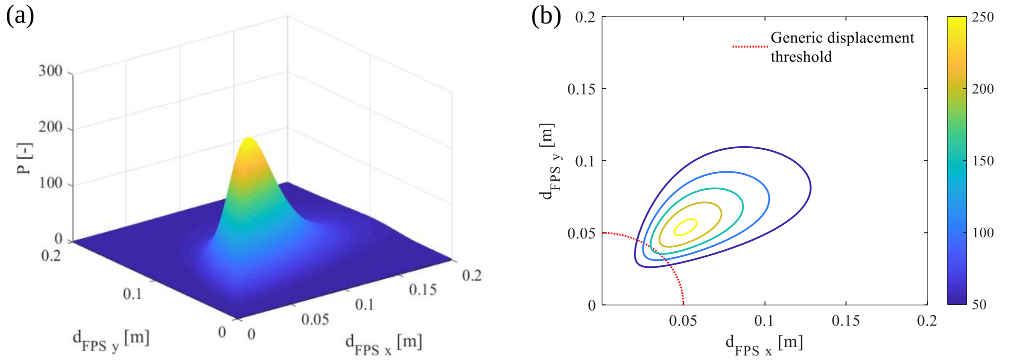

Figure 27. 3D view of the Joint PDF for the isolation system (a) and level curves (b) with a generic displacement threshold (with masonry infills).

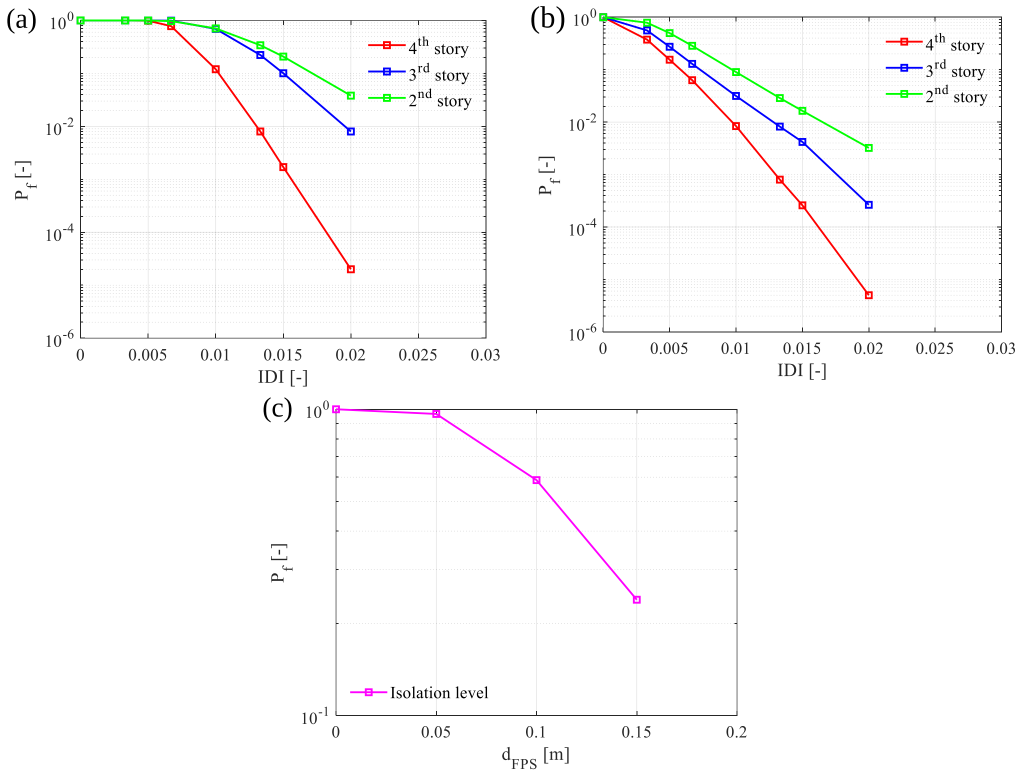

Figure 28. Probabilities of exceedance with bi-variate log-normal assumption in logarithmic scale: base fixed model (a); base isolated model (b); Isolator devices for base isolated model (c); (with masonry infills).

We can observe much higher probability of exceedance when the parameters *IDIs* and d_{FPS} are considered in both the planar directions of the building. This is mainly due to a good degree of correlation that always exists between the abovementioned parameters. Figures 25-28 shows how the presence of the infills leads to lower exceeding probabilities as well as a lower dispersion of the spatial response of the structure along the height, especially, for the fixed-base structure.

In conclusion, in the case of retrofitting intervention using FP devices, the mentioned above results turn out into a reduced damage level for fully operational (LS1) and operational (LS2) limit states enhancing the recovery of functionality after seismic events. Also, with reference to the life safety (LS3) and near-collapse (LS4) limit states, the interaction between FP isolation system and presence of infill wall reduces the probability exceeding the related limit states thresholds as well as the potential direct (i.e., casualties, recovery or rebuild of the structure) and indirect (i.e., loss of service of the building related to its function for community) costs.

5. Conclusions

The present investigation aims to analyze the efficiency, in probabilistic terms, of use of FPS with single concavity devices to retrofit an existing RC building with both in plane and in elevation irregularities. In particular, the interaction between the FP isolation system and the presence of irregular distribution of infilled frames have been discussed. Appropriate NL numerical models of the structure have been defined on the base of concentrated plasticity approach using fiber-hinges cross section for both fixed-base and base-isolated structure inclusive or not of the influence of masonry infills. Then, spatial NL dynamic simulations have been developed considering twenty-one natural seismic events with the three acceleration components.

The outcomes of the NL dynamic simulations highlight that the presence of the FPS isolators allow to reduce drastically the values of the IDIs limiting the occurrence of local failures of columns in shear. In particular, in the base isolated structure the shear failure in columns where partial infills are located are prevented in comparison to the fixed-base building. The presence of masonry infills improves the effectiveness of the isolation system by furtherly reducing the displacement demand. These abovementioned effects are then quantified in probabilistic terms by computing the lognormal distribution functions on the IDIs and on the relative displacement with respect to the ground of FPS isolators adopting both mono-variate and bi-variate approaches. As expected, the probabilities of exceedance show a significant drop between the fixed-base and the base-isolated building. This result is confirmed and even magnified by the structural effect of masonry infills highlighting the importance to account for their influence during seismic assessment of existing buildings. In fact, their contribution can be determinant to satisfy the performance requirements of current design codes without the need of strengthening intervention on structural members. In conclusion, further developments should be carried out in order to estimate seismic reliability of such kind of structure including the site-dependent seismic hazard investigating the contribution of infills to enhance its safety.

Author Contributions: "Conceptualization, D.G., E.M. and L.G.; methodology, D.G., E.M. and L.G.; software, D.G., E.M. and L.G.; validation, D.G., E.M. and L.G.; formal analysis, D.G., E.M. and L.G.; investigation, D.G., E.M. and L.G.; resources, D.G., E.M. and L.G.; data curation, D.G., E.M. and L.G.; writing—original draft preparation, D.G., E.M., L.G., G.C.M and P.C.; writing—review and editing, D.G., E.M., L.G., G.C.M and P.C.; visualization, D.G., E.M. and L.G.; supervision, D.G., E.M., L.G., G.C.M and P.C.. All authors have read and agreed to the published version of the manuscript."

Funding: This research received no external funding.

Data Availability Statement: Not applicable.

Acknowledgments:

This work is part of the collaborative activity developed by the authors within the framework of the Commission 3 – Task Group 3.1: *"Reliability and safety evaluation: full-probabilistic and semi-probabilistic methods for existing structures"* of the International Federation for Structural Concrete (*fib*).

This work is also part of the collaborative activity developed by the authors within the framework of the WP 11 – Task 11.4 – ReLUIS.

This work is also part of the collaborative activity developed by the authors within the framework of the "PNRR - VS3 "Earthquakes and Volcanos" - WP3.6".

Conflicts of Interest: The authors declare no conflict of interest.

References

1. Gino, D.; Castaldo, P.; Bertagnoli, G.; Giordano, L.; Mancini, G. Partial factor Bulletin 80: Assessment of an existing prestressed concrete bridge. *Structural Concrete* **2020**, *21*, 15–31, https://doi.org/10.1002/suco.201900231.
2. Clemente, P.; Buffarini, G.; Dolce, M.; Parducci, A. La scuola Angeli di San Giuliano: un esempio significativo di isolamento sismico. *Energ Ambiente Innov* **2009**, *3*, 107–116.
3. NTC18 - Aggiornamento delle nuove Norme tecniche per le costruzioni DM 17.01.2018. *Ministero delle Infrastrutture e dei Trasporti*, Italia.
4. EN 1998-1 – General rules, seismic actions and rules for buildings. *CEN European Committee for Standardization*, Bruxelles, Belgium.
5. Castaldo, P.; Mancini, G.; Palazzo, B. Seismic reliability-based robustness assessment of three-dimensional reinforced concrete systems equipped with single-concave sliding devices. *Engineering Structures* **2018**, *163*.
6. Mishra, S.K.; Roy B.K.; Chakraborty, S. Reliability-based-design-optimization of base isolated buildings considering stochastic system parameters subjected to random earthquakes. *Int J Mech Sci* **2013**, *75*, 123–133.
7. Valente, M.; Milani, G. Alternative retrofitting strategies to prevent the failure of an under-designed reinforced concrete frame. *Engineering Failure Analysis* **2018**, *89*, 271-285, https://doi.org/10.1016/j.engfailanal.2018.02.001.
8. Zou, X.K.; Wang, Q.; Li, G.; Chan, C.M. Integrated reliability-based seismic drift design optimization of base-isolated concrete buildings. *J Struct Eng* **2010**, *136*, 1282–1295.
9. Christopoulos, C.; Filiatrault, A. *Principles of Passive Supplemental Damping and Seismic Isolation*. IUSS Press, Pavia, Italy, 2006.
10. Su, L.; Ahmadi, G.; Tadjbakhsh, I.G. Comparative study of base isolation systems. *Journal of Engineering Mechanic* **1989**, *115*, 1976–1992.
11. Zayas, V.A.; Low, S.S.; Mahin, S.A. A simple pendulum technique for achieving seismic isolation. *Earthq. Spectra* **1990**, *6*, 317–333.
12. Castaldo, P.; Palazzo, B.; Della Vecchia, P. Seismic reliability of base-isolated structures with friction pendulum bearings. *Engineering Structures* **2015**, *95*, 80-93.
13. Castaldo, P.; Alfano, G. Seismic reliability-based design of hardening and softening structures isolated by double concave sliding devices. *Soil Dynamics and Earthquake Engineering* **2020**, *129*, 105930.
14. Briseghella, B.; Zordan, T.; Liu, T.; Mazzarolo, E. Friction Pendulum System as a Retrofit Technique for Existing Reinforced Concrete Building. *Structural Engineering International* **2013**, *23(2)*, 219-224, doi: 10.2749/101686613X13439149157759.
15. Mazza, F.; Mazza, M.; Vulcano, A. Base-isolation systems for the seismic retrofitting of r.c. framed buildings with soft-storey subjected to near-fault earthquakes. *Soil Dynamics and Earthquake Engineering* **2018**, *109*, 209–221.
16. Yang, T.; Bergquist, S.; Calvi. P.M.; Wiebe, R. Improving seismic performance using adaptive variable friction systems. S*oil Dynamics and Earthquake Engineering* **2021**, *140*, 106442.
17. Mazza, F.; Vulcano A. Nonlinear dynamic response of r.c. framed structures subjected to near-fault ground motions. *Bull Earthquake Eng* **2010**, *8*, 1331–1350, DOI 10.1007/s10518-010-9180-z.
18. Lupășteanu, V.; Soveja, L.; Lupășteanu, R.; Chingălată, C. Installation of a base isolation system made of friction pendulum sliding isolators in a historic masonry orthodox church. *Engineering Structures* **2019**, *188*, 369-381, DOI: 10.1016/j.engstruct.2019.03.040.
19. D'Amato, M.; Gigliotti, R.; Laguardia, R. Seismic Isolation for Protecting Historical Buildings: A Case Study. *Frontiers in Built Environment* **2019**, *5*, 87, DOI:10.3389/fbuil.2019.00087.
20. De Angelis, A.; Pecce, M.R. The Role of Infill Walls in the Dynamic Behavior and Seismic Upgrade of a Reinforced Concrete *Framed Building Frontiers in Built Environment* **2020**, *6*, 10.3389/fbuil.2020.590114.
21. Celarec, D.; Ricci, P.; Dolsek, M. The sensitivity of seismic response parameters of the uncertain modeling variables of masonry-infilled reinforced concrete frames. *Engineering Structures* **2012**, *35*, 165–177, 10.1016/j.engstruct.2011.11.007.
22. Celik, O.C. Effect of AAC infill walls on structural system dynamics of a concrete building. *J. Earthq. Eng.* **2015**, *20*, 738–748, 10.1080/13632469.2015.1104757.
23. Vasani, M.H.: Ramani, D. Comparative study of effect of infill walls on fixed base and base isolated reinforced concrete structures. *JETIR* ***2017***, *4(04)*, ISSN-2349-5162
24. Shiroll, S.; Kori, J.G. Seismic Base Isolation of RC Frame Structures with and without Infill. *International Research Journal of Engineering and Technology (IRJET)* **2017**, *04(06).*

25. SAP2000. *CSI Analysis Reference Manual: for SAP2000*. ETABS, SAFE and CsiBridge.
26. Gino, D.; Anerdi, C.; Castaldo, P.; Ferrara, M.; Bertagnoli, G.; Giordano, L. Seismic Upgrading of Existing Reinforced Concrete Buildings Using Friction Pendulum Devices: A Probabilistic Evaluation. *Appl. Sci*. **2020**, *10*, 8980; doi:10.3390/app10248980.
27. ESM Database. *European strong motion database*. http://www.isesd.hi.is/.
28. Bertero, R.D.; Bertero, V.V. Performance-based seismic engineering: the need for a reliable conceptual comprehensive approach. *Earthquake Eng. Struct. Dyn*. **2002**, *31*, 627–652. http://dx.doi.org/10.1002/eqe.146.
29. Aristomenis, V.; Tsantilis T.; Triantafillou, C. Innovative seismic isolation of masonry infills using cellular materials at the interface with the surrounding RC frames. *Engineering Structures* **2018**, *155*, 279–297.
30. Naeim, F.; Kelly, J.M. *Design of seismic isolated structures: from theory to practice*. John Wiley & Sons, Inc., 1999.
31. Constantinou, M.C.; Mokha, A.; Reinhorn, A.M. Teflon bearings in base isolation. II: Modeling. *J Struct Eng* **1990**;*116(2)*, 455–474.
32. Constantinou, M.C.; Whittaker, A.S.; Kalpakidis, Y.; Fenz D.M.; Warn, G.P. *Performance of seismic isolation hardware under service and seismic loading*. Technical report MCEER-07-0012, 2007.
33. Fardis, M.N.; Panagiotakos, T.B. Seismic design and response of bare and infilled reinforced concrete buildings – part II: infilled structures. *J Earthquake Eng* **1997**, *1(3)*, 473–503.
34. De Risi, M.T.; Del Gaudio, C.; Verderame, G.M. Evaluation of repair costs for masonry infills in RC buildings from observed damage data: the case-study of the 2009 L'Aquila earthquake. *Buildings* **2019**, *9*, 122; doi:10.3390/buildings9050122.
35. Guevara, L.T.; Garcia, L.E. The captive- and short-column effect. *Earthquake Spectra* **2005**, *21*.
36. Dolsek, M.; Fajfar, P. Mathematical modeling of an infilled RC frame structure based on the results of pseudo-dynamic tests. *Earthquake Eng. Struc.t Dynam.* **2002**, *31*, 1215–30.
37. Di Trapani, F.; Bertagnoli, G.; Ferrotto, M.F.; Gino, D. Empirical equations for the direct definition of stress–strain laws for fiber-section-based macromodeling of infilled frames. *J. Eng. Mech.* **2018**, *144(11)*, 04018101.
38. Scott, B.D.; Park, R.; Priestley, M.J.N. Stress–strain behavior of concrete confined by overlapping hoops at low and high strain rates. *ACI Journal* **1982**, *79(1)*, 13–27.
39. Castaldo, P.; Gino, D.; Bertagnoli, G.; Mancini G. Resistance model uncertainty in non-linear finite element analyses of cyclically loaded reinforced concrete systems. *Engineering Structures* **2020**, *211*, 110496,https://doi.org/10.1016/j.engstruct.2020.110496.
40. Castaldo, P.; Gino, D.; Mancini G. Safety formats for non-linear analysis of reinforced concrete structures: discussion, comparison and proposals. *Engineering Structures* **2019**, *193*, 136-153, https://doi.org/10.1016/j.engstruct.2018.09.041.
41. Mander, J.B.; Priestly, M.J.N.; Park, R. Theoretical stress-strain model for confined concrete. *Journal of Structural Engineering* **1988**, *114*(*8*), 1804-1826.
42. Saatcioglu, M.; Razvi, R.S. Strength and ductility of confined concrete. *Journal of Structural engineering* **1992**, *118(6)*, 1590–1607.
43. EN 1992-1-1: *Eurocode 2 – Design of concrete structures. Part 1-1: general rules and rules for buildings*. CEN, Brussels, 2014.
44. McKenna, F.; Fenves, G.L.; Scott, M.H. *Open system for earthquake engineering simulation*, University of California, Berkeley, CA, 2000.
45. Priestley, M.J.N.; Park, R. Strength and ductility of concrete bridge columns under seismic loading. *ACI Struct. J.* **1987,** *84(1)*, 61-76.
46. Takeda, T.; Sozen, M. A.; Nielsen, N.N. Reinforced Concrete Response to Simulated Earthquakes. *J. Struct. Engrg*. *Div. ASCE* **1970**, *96(12)*, 2257–2273.
47. EN 1990. *Eurocode – Basis of structural design*. CEN, Brussels, Brussels.
48. European strong motion database (ESM). http://www.isesd.hi.is/
49. Hilber H.M.; Hughes, T.J.R.; Taylor, R.L. Improved numerical dissipation for time integration algorithms in structural dynamics. *Earthquake Engineering and Structural Dynamics* **1977**, *5*.
50. Cheng, F.Y. *Matrix analysis of structural dynamics: applications and earthquake engineering*. 2001
51. Faber, M.H. *Statistics and Probability Theory*. Springer, 2012.